Effects of Odd–Even Side Chain Length of Alkyl-Substituted Diphenylbithiophenes on First Monolayer Thin Film Packing Structure

Citation

Published Version

Permanent link

Terms of Use

Share Your Story

Accessibility

SUPPORTING INFORMATION FOR

Effects of Odd-Even Side Chain Length of Alkyl-Substituted Diphenyl-bithiophenes on First Monolayer Thin Film Packing Structure

Hylke B. Akkerman[1,6], Stefan C. B. Mannsfeld[2], Ananth P. Kaushik[3], Eric Verploegen[1,2], Luc Burnier[3], Jonathan D. Saathoff[3], Arjan P. Zoombelt[1], Sanghyun Hong[1,5],Sule Atahan-Evrenk[4], Xueliang Liu[4], Alán Aspuru-Guzik[4], Michael F. Toney[2], Paulette Clancy[3] and Zhenan Bao[1,*]

1. Stanford University, Department of Chemical Engineering, Stauffer III, 381 North-South Mall, Stanford, CA 94305-5025, USA.

2. Stanford Synchrotron Radiation Laboratory, 2575 Sand Hill Rd, Menlo Park, CA 94025, USA

3. Cornell University, School of Chemical and Biomolecular Engineering, 120 Olin Hall, Ithaca, NY 14853-5201, USA.

4. Harvard University, Department of Chemistry and Chemical Biology, 12 Oxford Street, Cambridge, MA 02138, USA

5. Current address: Samsung Cheil Industries, Chemicals R&D Center, Gochun-Dong, Uiwang-Si, Gyeonggi-Do, Korea

6. Current address: Holst Centre, High Tech Campus 31, 5656AE, Eindhoven, The Netherlands

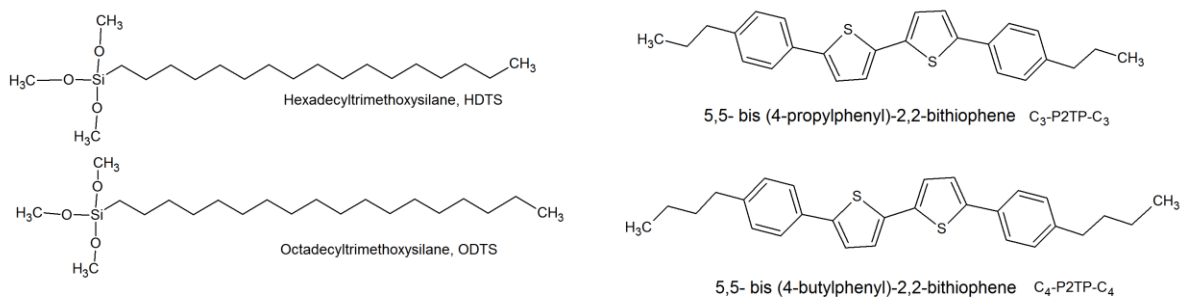* Email: zbao@stanford.edu

1. Chemical structures

Figure S1. Chemical structures of the molecules for the SiO_2 treatment, HDTS and ODTS, and two molecules from the C_N-P2TP-C_N series are shown, with $N = 3$ and 4.

2. Characterization of heptadecyltrimethoxysilane (HDTS) and octadecyltrimethoxysilane (ODTS) self-assembled monolayers.

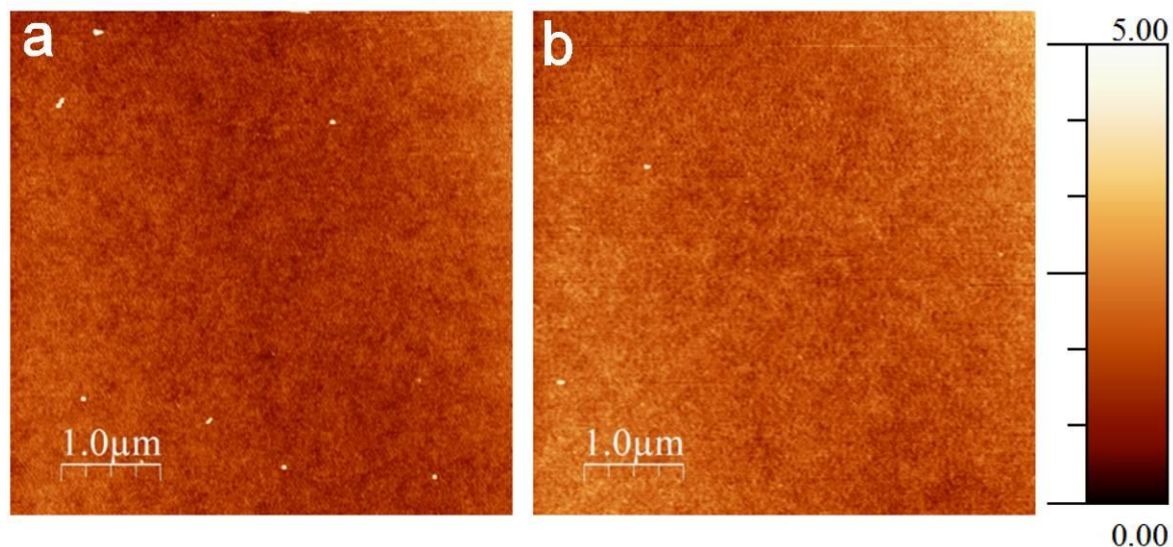Figure S2. AFM images of crystalline self-assembled monolayers of HDTS (a) and ODTS (b) on SiO_2. The root-mean-square roughness (5×5 μm area) for both monolayers is 0.38 nm RMS and 0.37 nm RMS for HDTS and ODTS, respectively.
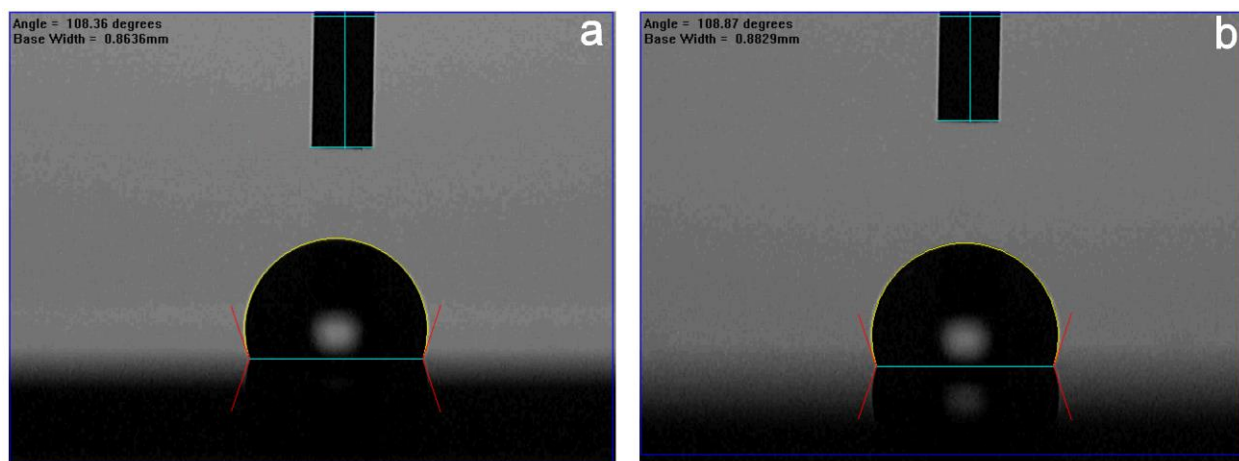

Figure S3. Water contact angle measurements of the HDTS (a) and ODTS (b) self-assembled monolayers on SiO_2. The contact angle is 109.3° ± 1.4° for HDTS and 108.4° ± 0.6° for ODTS.

3. The influence of substrate temperature on the apparent grain size of P2TPs

The effect of substrate temperature on grain size was determined by thermally evaporating a half covered monolayer of C_8-P2TP-C_8 on ODTS at substrate temperatures ranging from room temperature to 115 °C. A large increase in grain size is observed (Figure S4), indicating substrate temperature as a large contributor to the increase in grain size.
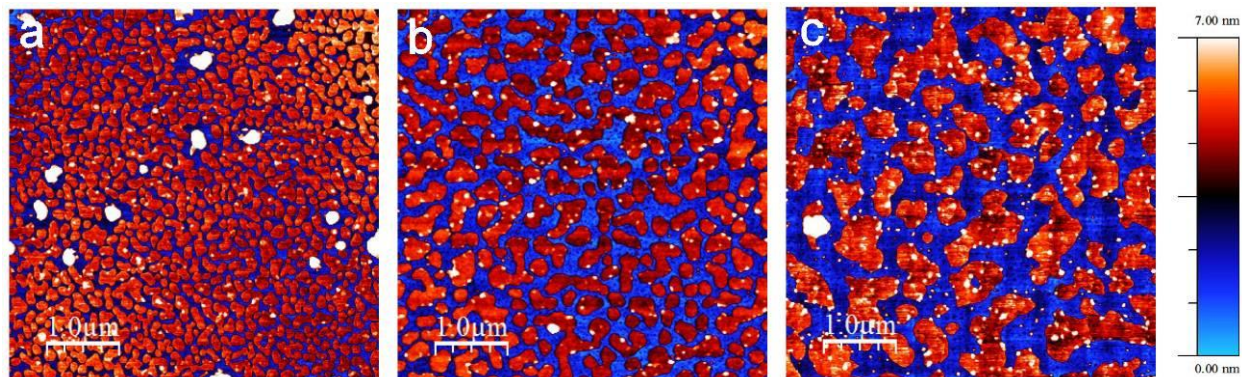
Figure S4. AFM images of the first layer of C_8-P2TP-C_8 on ODTS, thermally evaporated at room temperature (a), 84 °C (b), and 115 °C (c). An increase in grain size with increasing substrate temperature is observed.

To see the effect of side chain length on the grain size, we evaporated the series of P2TP molecules on ODTS at 60 °C with a film thickness of 40 nm (Figure S5). Towards longer side chain length, the grain size increases and becomes more irregular in shape. This indicates a stronger 2 dimensional growth mode due to a decrease in interaction of the conjugated core with the underlying layers. Although we did not investigate the grain size versus chain length for the first layer of molecules for the complete series of P2TP, we strongly suspect this will result in a similar trend.

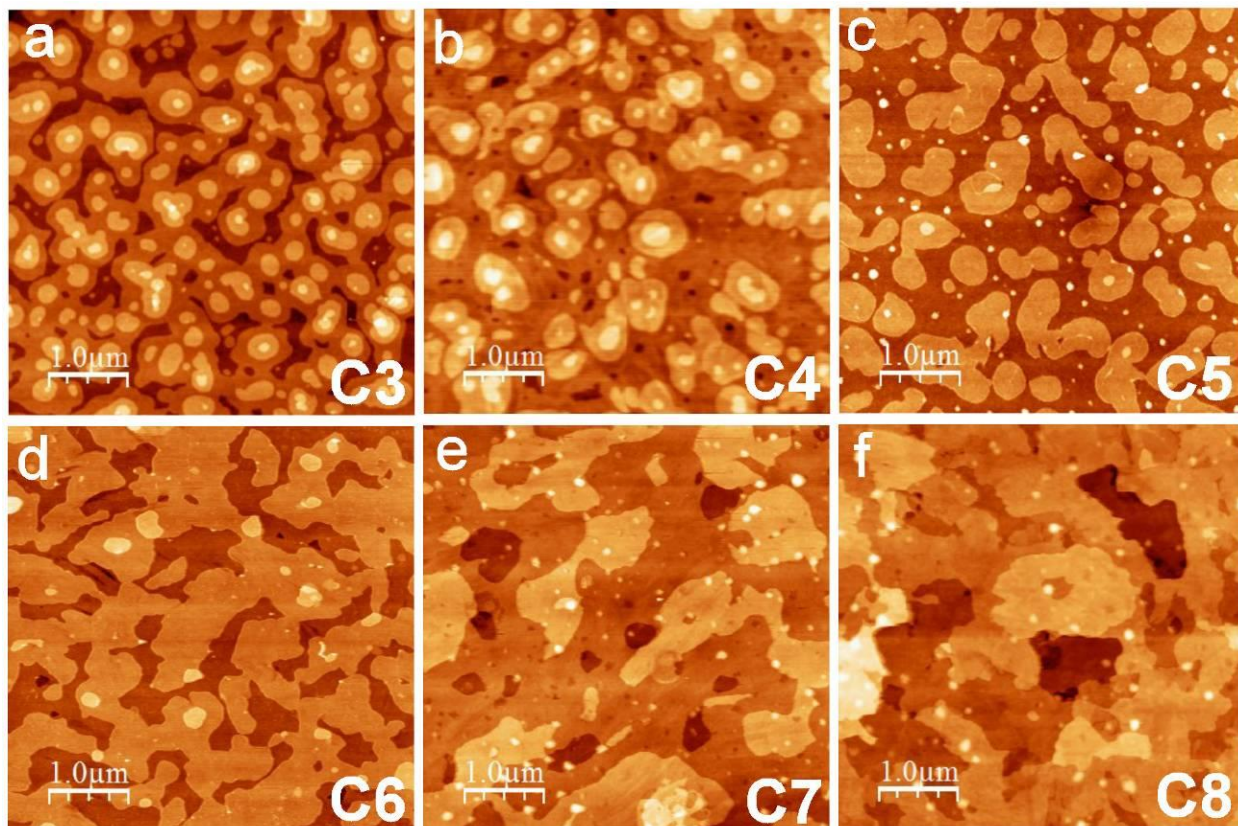Figure S5. AFM images of 40 nm thick films of C_N-P2TP-C_N, with N = 3−8, on ODTS. An increase in grain size is observed for longer side chains due to a decreased interaction of the conjugated core with the underlying layers, or substrate.

4. Grazing incidence X-ray diffraction

The motif by which the molecules pack inside the C_N-P2TP-C_N unit cells was extracted by crystallographic refinement of the diffraction intensity obtained from the Bragg rods. This was achieved by fitting theoretically calculated diffraction intensities to the measured intensity data, assuming scattering from a smooth thin film is kinematical. Besides a correction for the beam polarization (95% in-plane polarized), additional multiplicative corrections needed to be applied to the theoretical diffraction intensity values $I_{hk}(q_z) \sim |F_{hk}(q_z)|^2$. Even though our GIXD setup involves no rotation of either detector or sample, a Lorentz correction, $1/\cos(\theta)\sin(\theta)\cos(\theta)$, is necessary because the film forms a 2D-powder in the substrate surface plane. For simplicity, we assumed an isotropic molecular mean square displacement $\langle U^2 \rangle$, for the Debye Waller factor, $\exp(-\langle U^2 \rangle q^2)$. It is important to realize that the correct total peak intensity is recorded in the uncorrected images. The angular dependence of the atomic scattering factors was calculated using a Cromer-Mann function and corresponding coefficients. The coefficients for the hydrogen factor were obtained by fitting literature data to a Cromer-Mann function. The energy-dependent real and complex corrections to the scattering factors were taken from literature.

The alignment of the two C_N-P2TP-C_N molecules in the determined monolayer unit cell was extracted from the GIXD peak intensities by numerical optimization of the crystallographic residual that fits the corrected theoretical diffraction intensities along the Bragg rods to the experimentally obtained intensity data. Integrated intensity values were measured at 40 different values of q_z between q_z=0.05…0.4 Å^{-1} along the first five Bragg Rods in GIXD images of a sub-monolayer C_N-P2TP-C_N films after background removal. In these GIXD images, the {01} and {10} rods are completely extinct which is indicative of p2gg symmetry (two glide-symmetry planes create systematic absences of peaks). Therefore, the respective experimental $I_{10}(q_z)$ and $I_{01}(q_z)$ values were set zero and included in the fit at five different q_z values.

5. Computer Simulations

5.1 Configuration of the system

In the experimental set up, molecules that form surface coatings, like the ODTS Self-Assembled Monolayers (or SAMs), are deposited on an amorphous silicon dioxide substrate. The head group, consisting of three chlorine atoms, reacts with the -OH groups of the substrate, forming an -O-Si bond that tethers the molecule to the surface. To emulate this in the simulation, we tethered each SAM molecule to an *x-y* location in space. Since the ODTS ligands are relatively long (~2.3 nm), an explicitly modeled surface beneath the SAM is unnecessary. The ODTS SAM molecules were tethered to hexagonal lattice points in free space at the oxygen atom, *i.e.*, the position of the oxygen atom was fixed throughout the simulation. This choice followed experimental evidence that suggests the oxygen atoms are attached to the substrate surface, thereby anchoring the SAM molecules at this point. It is possible that, on real surfaces, the SAM molecule could be tethered *via* more than one oxygen atom in the head group, which implies that the silicon atom of the head group is also essentially fixed in place [1]. To study the impact of this eventuality and better define an appropriate initial system configuration, we conducted simulations in which *both* the silicon and oxygen atoms were fixed in place. The energetics of the system differed by less than 5% in energy and with no observable structural difference in the system whether just oxygen was fixed, or both oxygen and silicon were fixed. Thus all the remaining simulations described in this paper assumed that the SAM molecule is tethered to the substrate by one oxygen atom.

The simulation set-up used ODTS's preferred hexagonal lattice; here, 98 SAM molecules, consisting of 7x7 unit cells with two molecules per unit cell. This involves the consideration of 5,928 atoms for the ODTS molecules alone. The characteristic lattice parameter of the hexagonal packing was chosen to match the packing density determined from X-ray diffraction measurements [2]. The oxygen atoms are fixed to simulate the binding of the ODTS with the substrate. After thermalizing at 300 K, the simulation shows that the tilt angle of ODTS is strongly correlated to the SAM density, as shown in Table S1.

Simulation and experimental values for the tilt angle agree well (6° and 7°, respectively) at the experimental density of 5 molecules/nm^2. This density was used throughout the simulations.

Density (molecules/nm^2)	3	4	5
Tilt (degrees)	30 ± 2	22 ± 2	6 ± 2

Table.S1: MD simulation-predicted average tilt angle (degrees) of ODTS for different densities (molecules/nm^2)

We determined that the ODTS molecules could be fixed in place during the simulation without loss of accuracy of the surface topography and subsequent morphology of P2TP molecules. This simplification is possible because the movement of individual SAM molecules is limited at this high density. The advantage of fixing the molecules is that it allows a very significant reduction in computational expenditure without loss of accuracy.

All the molecules used in the simulation (ODTS and P2TP) were created using the Molden software package [3] and an energy minimization of the initial guessed structures was performed using a standard minimization algorithm - the limited memory L-BFGS minimization using a modified version of the algorithm of Nocedal which is a part of the TINKER software package [4].

The next task is to determine the lowest energy configuration of a unit cell of two P2TP molecules, as a starting point for the simulations. Since the preferred P2TP orientation in the unit cell for the force field model chosen in this study is not known *a priori*, we had to investigate the effect of the angle between each molecule on the energy of the system, as shown in Figure S6. The maximum in energy corresponds to a completely eclipsed configuration (at ~270°). We observed two minima that are close in energy (-9 and −7.5 kcal/mole) at 240° and 300°, separated by a large energy barrier (of ~45 Kcal/mole). These minima are for two isolated molecules interacting with each other and do not necessarily represent the true global minima in energy for a bulk 2D lattice. This necessitated two separate sets of simulations,

described below, to determine the configuration that gives rise to the lower energy in the *bulk* 2D lattice with periodic boundary conditions. Such a study found that the lower energy minimum for the bulk lattice occurred at an angle of 300°.
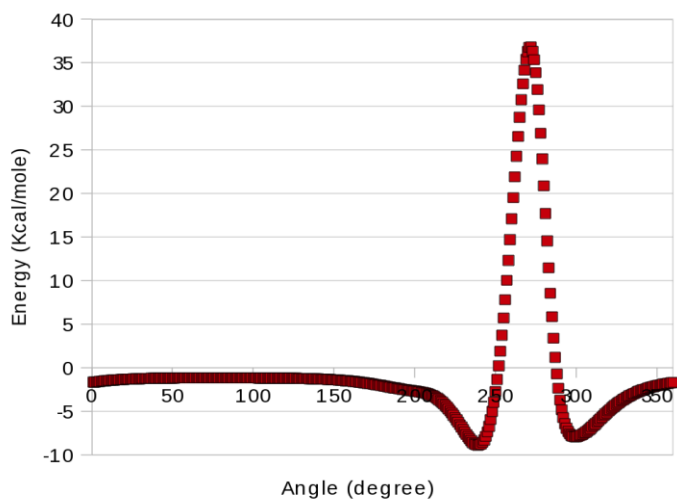

Figure S6: Energy as function of the angle between two molecules.

The intermolecular distance at the energy minimum defines both the lattice parameters and the density of the monolayers. The first simulation runs performed a cursory fit allowing the energy to be minimized; this was determined by keeping one molecule fixed and moving the other molecule relative to the fixed molecule in the x and y directions. For example, for C3-P2TP-C3, the energy dependence on the distance is as shown in Figure S7. For each distance, the molecules were rotated and a minimum in the energy was found. The net results of minimizing both the distance and angle leads to the optimum configration of the molecles in the unit cell.
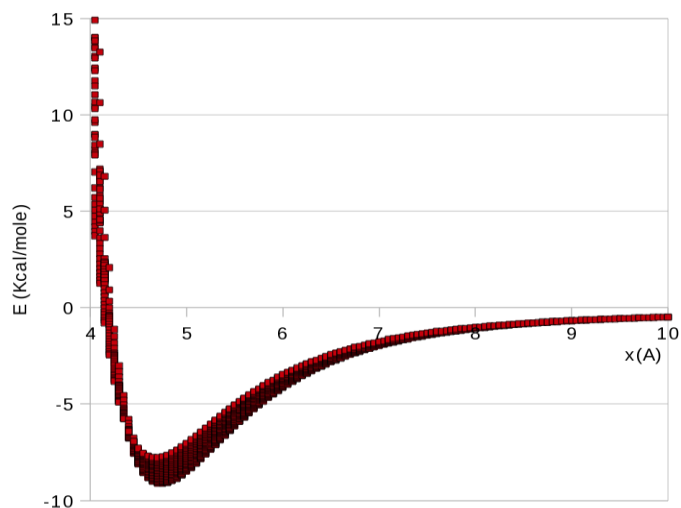
Figure S7. Energy as a function of the distance along the x axis between two molecules. For every value of x, the second molecule is moved along the y-axis. For every x-value, there are several values of energy corresponding to positions along the y-axis. In this way, the minimum along both x- and y-axes are found. The graph (Figure S7) is plotted for E as a function of x alone.

The optimized configuration of the square lattice of the P2TPs consists of two molecules, rotated by 300° in relation to each other, and characterized by lattice parameters that are dependent on the chain length of the molecule. Figure S8 represents the optimum configuration of the molecule for n=3 and n=4.
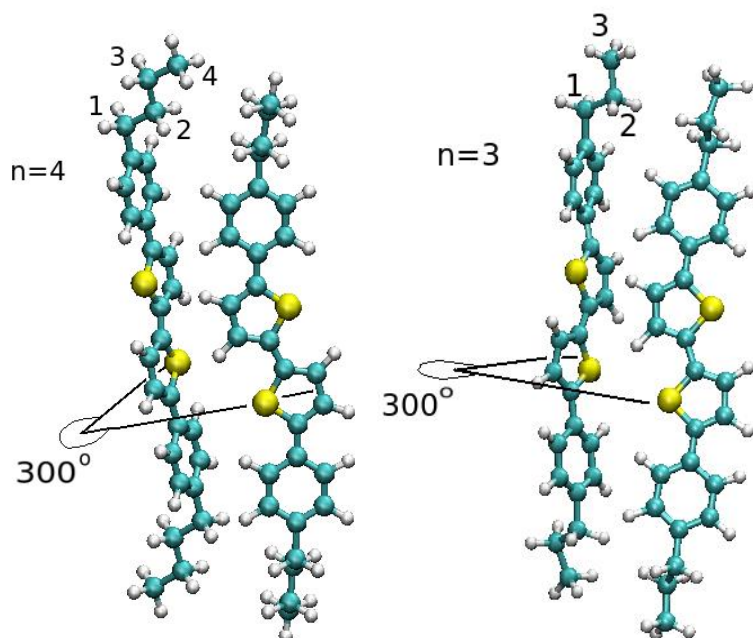
Figure S8. Left: molecule C3-2P2TP-C3 / Right: molecule C4-2P2TP-C4 after optimization.

Once the minimized configuration for the two molecules in the unit cell was obtained, a larger lattice consisting of several unit cells with this molecular configuration was constructed to represent the experimental set-up of a layer of P2TP molecules deposited on the ODTS surface. The lattice consisted of around 70 P2TP molecules (3,080-4,130 atoms for the different chain lengths studied) arranged on top the ODTS SAM layer. The system was then equilibrated as given in the section describing the simulation details below.

5.2 Intermolecular Potential Models

The choice of intermolecular potential model is a very important part of a molecular simulation. We chose to use the non-reactive semi-empirical MM3 potential to model all the SAM-SAM and P2TP-SAM interactions. The MM3 potential has been shown, by us and others [5-8], to describe, quite accurately, hydrocarbons [5], fluorinated hydrocarbons [7] and multiply ringed molecules of the type we studied here. MM3 incorporates stretching, bending, and torsional energies, as well as the van der Waals

interaction energies based on phenomenologically determined parameters. The total energy may be represented as follows:

$$E = E_b + E_a + E_{tor} + E_{aa} + E_{sb} + E_{stor} + E_{vdw}$$

with

$$E_{vdw} = A exp\left\{-{}^r/_\rho\right\} + {}^C/_{r^6}$$

where E_b is the bond-stretch, E_a is the angle-bend, E_{tor} is the torsion, E_{aa} is the bend-bend, E_{sb} is the stretch-bend and E_{stor} is the stretch-torsion potential. The potential does not involve electrostatic interactions. The intermolecular van der Waals interactions take the form of a Buckingham potential modified with tapering polynomials so that the energy may smoothly decrease to zero at a cut-off distance of 9Å.

We have used this model extensively to study the energetics and structural characteristics of an array of small organic semiconducting molecules including the acenes, rubrene, DIP, sexiphenyl and C_{60} [9, 10] and have confidence in its ability to model conjugated systems. For instance, we conducted an extensive survey of twelve Density Functional Theory models, as well as the MM3 and MM3-π models for biphenyl and eight models (four DFT and four semi-empirical models) for the sexiphenyl molecule. We found virtually all the models to give consistent energetically preferred structures [11]. Both MM3 models (with and without an additional term to represent pi-bonding) represented the behavior of sexiphenyl and biphenyl molecules with quantitative accuracy compared to the DFT models. Based on our studies and those of the Allinger group, we are confident in the ability of MM3 to be sufficiently accurate to describe P2TP molecules on a SAM surface without having to resort to using MM3-π, a variant of MM3 which is more accurate for molecules with an extensive π-electron system but which is about 20 to 100 times slower in execution time.

5.3 Simulation Details

The time evolution of the system was followed using a simulation approach using the Modified Beeman Algorithm as part of the TINKER software package. As mentioned above, optimized structures of the SAM molecules and the P2TP molecule were obtained from an energy minimization of an initial guess structures using a standard minimization algorithm, here, the limited memory L-BFGS minimization using a modified version of the algorithm of Nocedal [12]. The system consisted of the hexagonally packed ODTS layer underneath, and a P2TP layer arranged in a herringbone lattice on top of the ODTS. The system was first thermalized at 300 K using a Nosé-Hoover thermostat in the canonical (NVT) ensemble for a period of ~100 ps with a time step of 1.0 fs (*i.e.*, 100,000 time steps) in order to suppress significant fluctuations in temperature and equilibrate the system.

The bottom ODTS layer was now frozen and the top P2TP layer was subject to an isothermal-isobaric (NPT) ensemble in order to determine the optimum lattice constant. The system was run for about 100,000 time steps corresponding to ~100 ps. Once the system was equilibrated under NPT, the time-averaged and spatially averaged lattice constant was calculated and, with this mean lattice constant fixed, the system was once again subjected to the NVT ensemble for another period of equilibration. The equilibration time was again around ~100 ps.

After equilibration was complete, the average tilt angle of the P2TP layer above the ODTS SAM layer was measured. The tilt angle was calculated as the angle made by the vector made by the backbone of the P2TP molecule with the normal to the surface of the film. This is in agreement with the manner in which the tilt angle was calculated experimentally. The tilt angle was then compared with experiment and observed to vary as a function of the side chain length of the P2TP molecule as described in the results section of the main article.

To compare the optimized structure of the P2TP molecules in the presence or absence of the underlying SAM, we adopted a similar simulation procedure to that mentioned above, but without the presence of the SAM. The energy-minimized structure of the series of P2TP molecules with different alkane chain lengths were used as mentioned above: The simulation box was set up such that no SAM was present, and that sufficient vacuum existed above and below the 2D P2TP crystal so that periodic images would not interact and the system represented a thin film of the P2TP molecules. The initial 100 ps NVT step used above was omitted because there was no SAM layer that needed to be equilibrated. The following NPT step was extended to 400 ps because additional time was needed for the box to equilibrate with the SAM removed. This NPT step (in which the volume can vary) allowed the lattice parameters to change to further optimize the unit cell. The final 100 ps NVT step, as well as the angle measurements and equilibrated unit cell parameters, were carried out as described above.

The results for the preferred tilt in the absence of the SAM show that the odd-even effect persists in the absence of the SAM, but is diminished. This result shows that the odd-even effect is partially caused by the preferred packing of the P2TP molecule itself, but significantly enhanced by the interaction of the P2TP molecules with the SAM.

Note that comparing the absolute value of the tilt angles produced by MD and experiment should be done with care. The tilt angle value in the simulations depends on whether you measure the angle of the molecule as that formed by a line taken from the bottom to the top of the molecule, in comparison to the substrate (or, in the absence of the SAM, the horizontal baseline of the average molecular positions) or whether you choose to use only the fairly rigid central core formed by the thiophene section, and not the include the alkyl chains at either end of the molecule. However, regardless of which method you adopt, the odd-even phenomenon persists.
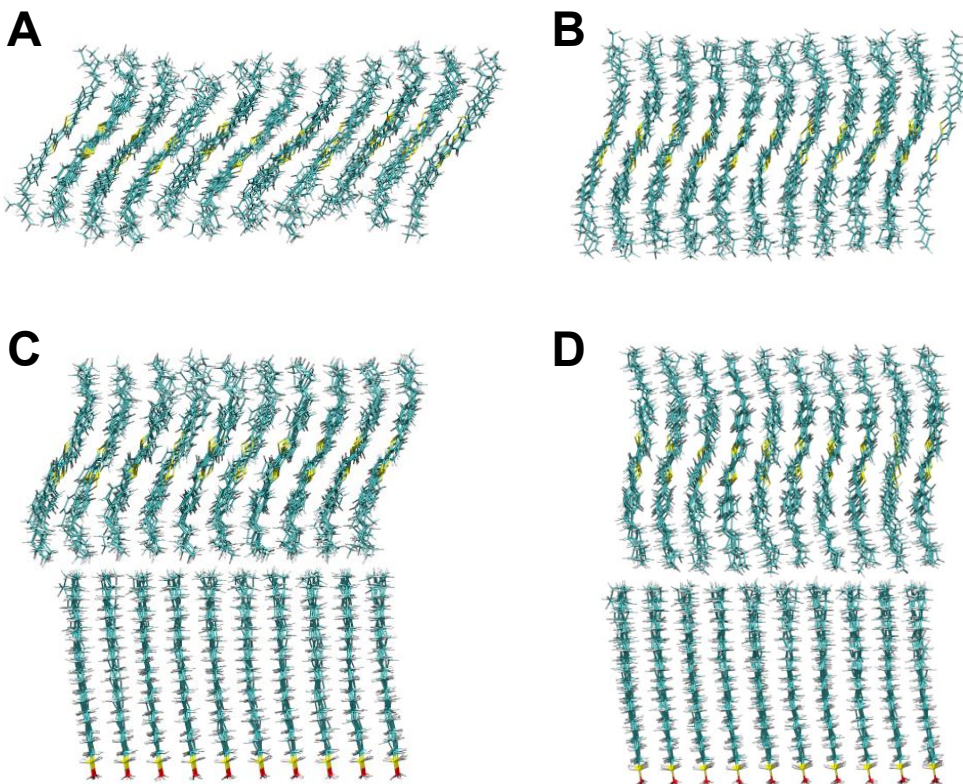
Figure S9. Representative images of the MD simulations that demonstrate the odd-even effect and the effect of having a SAM in contact with the P2TP crystal. The images are as follows: **A** shows the even C_4-P2TP-C_4 2D crystal and **B** shows the odd C_5-P2TP-C_5 2D crystal in the absence of a SAM. **C and D** show the C_4-P2TP-C_4 and C_5-P2TP-C_5 crystals on an ODTS SAM layer.
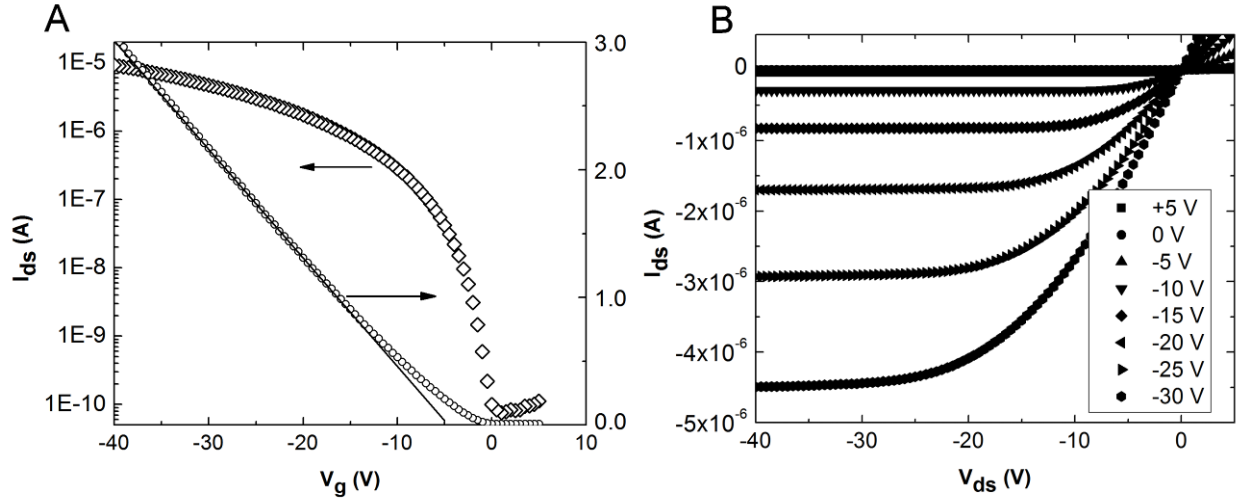
6. Transfer characteristics FETs

Figure S10 Transfer characteristics (V_{ds} = -40 V) (**A**) and output characteristics (**B**) of a FET fabricated with C_3-P2TP-C_3 on HDTS. The saturated mobility was determined from the slope of $I_{ds}^{1/2}$ versus Vg. The mobility was μ = 6.5×10^{-2} cm^2/Vs, with a threshold voltage V_t = -5 V (intersection linear fit and x-axis) and an on/off ratio of about 1×10^5.

The saturated field effect mobility was calculated by taking the slope of $I_{ds}^{1/2}$ versus V_g, as shown in Fig. S10. The intersection of the slope with the x-axis (I_{ds} = 0) determines the threshold voltage V_t. We used the following equation for calculating the mobility μ:

$$| I_{ds} | = \mu \cdot C_d \cdot \frac{W}{2L} \cdot (V_g - V_t)^2,$$

where C_d is the capacitance per unit area of the dielectric with a thickness d, W the width of the electrodes and L = the distance between source and drain electrode.

REFERENCES

[1]   H. Yamamoto, K. Nishiyama, and I. Ohdomari,, *J. Phys. IV*, **132**, 189 (2006).

[2]   Y. Ito, A. A. Virkar, S. C. B. Mannsfeld, J. H. Oh, M. Toney, J. Locklin, and Z. Bao, *J. Am. Chem. Soc.*, **131**, 9396 (2009)

[3]   Q. Yuan, S. C. B. Mannsfeld, M. L. Tang, M. F. Toney, J. Luning and Z. Bao, *J. Am. Chem. Soc.*, **130**, 11, 3502 (2008).

[4]   G.Schaftenaar and J. Noordik, *J. Comput. Aided Mol. Design*, **14**, 123 (2000).

[5]   J. W. Ponder, Tinker - software tools for molecular design, http://dasher.wustl.edu/ tinker/ (2010).

[6]   N. L . Allinger, Y. H . Yuh, and J.-H. Lii, *J . Am. Chem. Soc.*, **111**, 8576 (1989).

[7]   K.-H. Chen, J.-H. Lii, G. A. Walker, Y. Xie, H. F. S. III, and N. L. Allinger, *J. Phys. Chem A*, **110**, 7202 (2006).

[8]   K.-H. Chen, G. A. Walker, and N. L. Allinger, *Journal of Molecular Structure (Theochem)*, **490**, 87 (1999).

[9]   J. E. Goose and P. Clancy, *J. Phys. Chem. C*, **111**, 43- (2007).

[10]   R. Cantrell and P. Clancy, *Surface Science*, **602**, 3499 (2008).

[11]   J. E. Goose, E. L. First, and P. Clancy, *Phys. Rev. B*, **81**, 205310 (2010).

[12]   J. Nocedal, *Mathematics of Computation* **35**, 773 (1980).